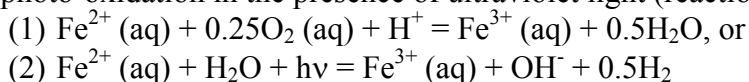


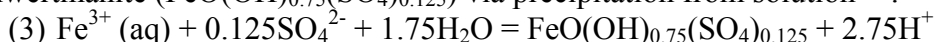
## 1.0 ACID TITRATION CALCULATIONS

We performed a set of calculations that allow us to assess the acid titrating capacity of Meridiani Planum outcrop relative to the amount of acid that would have been generated during the formation of the measured concentration and distribution of Fe<sup>3+</sup>-bearing mineral phases. The results of these calculations are summarized on **Table 1** of the manuscript. Our calculations are based on the set of alpha-particle X-ray spectrometer (APXS) analyses for which corresponding Mössbauer data was collected<sup>1-4</sup>. These data resolve both the bulk elemental composition and Fe-mineral distribution in outcrop. To avoid the effects of surface alteration rinds and adhering basaltic dust, we used data for analyses collected on outcrop targets abraded with the Rock Abrasion Tool<sup>5</sup>. These chemical and mineralogical data are shown on **Table S1**.

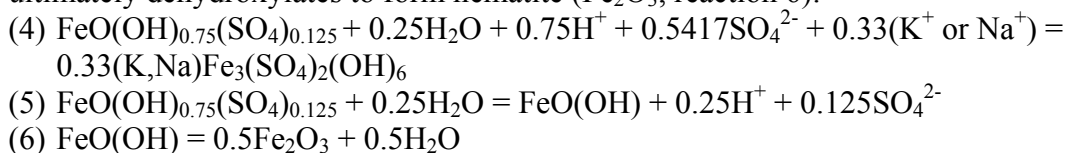
We assume that Fe<sup>2+</sup> was oxidized either by dissolved molecular O<sub>2</sub> (reaction 1), or by photo-oxidation in the presence of ultraviolet light (reaction 2):



We then assume that all dissolved Fe<sup>3+</sup> initially precipitated to form the mineral phase schwertmannite (FeO(OH)<sub>0.75</sub>(SO<sub>4</sub>)<sub>0.125</sub>) via precipitation from solution<sup>6,7</sup>:



We then assume that schwertmannite dissolves and re-precipitates to form a mixture of jarosite ((K,Na)Fe<sub>3</sub>(SO<sub>4</sub>)<sub>2</sub>(OH)<sub>6</sub>, reaction 4) and goethite (FeO(OH), reaction 5), which ultimately dehydroxylates to form hematite (Fe<sub>2</sub>O<sub>3</sub>, reaction 6):



Our titration methodology is best illustrated by way of example. On **Table S1**, Sample #1 (McKittrick\_RAT, APXS analysis collected on sol 31 of the *Opportunity* mission) has total Fe and SO<sub>4</sub> contents of 2.30 moles/kg and 2.66 moles/kg, respectively. The number of moles of Fe that are associated with schwertmannite (Fe3D3 on **Table S1**, discussed below), hematite, and jarosite is calculated by multiplying this Fe-concentration by the fractional Mössbauer subspectral areas reported for this rock analysis, in this case 0.22, 0.39, and 0.26 respectively. This calculation results in 0.51 moles Fe/kg in schwertmannite, 0.90 moles Fe/kg in hematite, and 0.60 moles Fe/kg in jarosite.

Next, we determine the number of moles of acid and sulfate produced or consumed in reactions 1-6. For each oxidation reaction (1 and 2), 1 mole of acid is consumed, either by direct consumption to form H<sub>2</sub>O (reaction 1), or by reaction with OH<sup>-</sup> (reaction 2), resulting in -1 moles of H<sup>+</sup>. For the formation of schwertmannite, a cumulative H<sup>+</sup> production of 1.75 moles is indicated, with 0.125 moles of SO<sub>4</sub><sup>2-</sup> consumed (i.e., (reaction 1 or reaction 2) + reaction 3). For the formation of jarosite, a cumulative H<sup>+</sup> production of 1 mole is indicated, with 0.667 moles of SO<sub>4</sub><sup>2-</sup> consumed ((r1 or r2)+r3+r4). For the

formation of hematite, a cumulative  $H^+$  production of 2 moles is indicated, with 0 moles of  $SO_4^{2-}$  consumed ( $(r1 \text{ or } r2)+r3+r5+r6$ ). The net acid production for this set of reactions is 4.75 moles  $H^+$ , and the net  $SO_4^{2-}$  consumption is 0.79 moles. Note that all of our calculations are written such that they are balanced on one mole of Fe; in this way they can be compared directly to the Mössbauer subspectral areas.

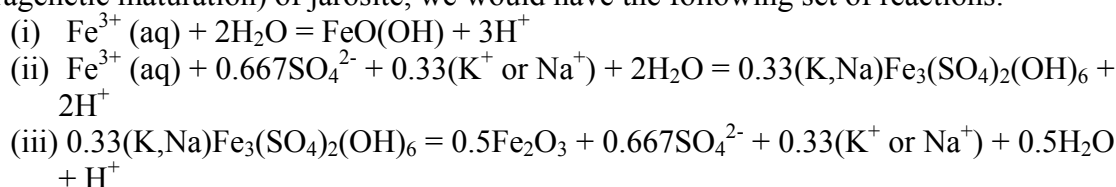
These values are then multiplied by the number of moles of Fe associated with each mineral phase in sample McKittrick\_RAT to determine the amount of  $H^+$  that was produced by oxidation and formation of the observed mineral distribution. The resulting values are 0.89 moles  $H^+$ /kg for schwertmannite (or Fe3D3), 1.80 moles  $H^+$ /kg for hematite, and 0.60 moles  $H^+$ /kg for jarosite, for a total acid production of 3.29 moles  $H^+$  per kg outcrop having the chemical and mineralogical composition of McKittrick\_RAT. The same calculation is performed for the  $SO_4^{2-}$ , resulting in a total of 0.46 moles  $SO_4^{2-}$  consumed per kg outcrop. For the purposes of our acid titration calculation (below) this  $SO_4^{2-}$  value is subtracted from the bulk concentration of  $SO_4^{2-}$  in outcrop since this  $SO_4^{2-}$  is effectively locked up in schwertmannite and jarosite, and is therefore unavailable to titrate  $H^+$  in solution. The results of our calculations for all APXS-Mössbauer analyses considered in this study are shown on **Table S2**.

Next, we calculate how much of the acid produced by  $Fe^{3+}$ -mineral formation can be titrated against the base anions ( $SO_4^{2-}$ ,  $Cl^-$ ,  $PO_4^{3-}$ ,  $CO_3^{2-}$ ) available in outcrop (**Table S1**). Because the acid titrating properties of these bases are strongly dependent on pH (**Figure S1**), we need to specify a range in pH values appropriate for determination of the base anion species distribution against which acid will be titrated. Fortunately, the presence of jarosite constrains our range to approximately pH = 2-4 (ref. 8-10). This observation allows us to perform two endmember calculations for the most (pH = 2) and least (pH = 4) acidic conditions. Once the relative proportions of the variously protonated base species are determined (**Figure S1**), we simply subtract (or titrate) the appropriate number of moles of  $H^+$  from our  $H^+$  production calculation to form those protonated base species. The  $\Delta G_f^\circ$  data on which **Figure S1** is based are valid at 25°C and 1 bar (STP), therefore our acid titration calculations are strictly valid only for these conditions. The results of these calculations for our pH = 2 and pH = 4 case are shown on **Tables S3** and **S4**, respectively, and indicate that for all outcrop analyses, there is a net excess of acid ( $H^+$ ) after titration. The acid generated would have been available to react with primary mineral phases (e.g., materials analogous to the basaltic sand that covers the present-day Meridiani surface) or with deeper lithologies if acidic waters retreated into the subsurface, in a manner analogous to that suggested by refs. <sup>11,12</sup>.

Below pH = 1.7, the acid titrating capacity of the outcrop begins to exceed  $H^+$  production. For instance, at pH = 1.6, the analysis Ontario\_London\_RAT has -0.1 moles of  $H^+$  remaining after titration against all available base. The excess acidity limit of pH=1.7 is conservative because we have assumed a high concentration of carbonate (1.4 weight %  $CO_3^{2-}$ ) in outcrop. The APXS does not detect elements lighter than Na and so our assumption for the carbonate content of the outcrop is based instead on the modeling of ref. 13 who report a maximum permissible  $CO_3^{2-}$  content for average Meridiani Planum outcrop of 1.4 weight %  $CO_3^{2-}$  (or 2.3 weight %  $CaCO_3$ ). On the basis of linear unmixing of data from the miniature thermal emission spectrometer, ref. 14 suggest that the actual  $CaCO_3$  content of average Meridiani Planum outcrop is more than likely lower than the upper limit reported by ref. 13.

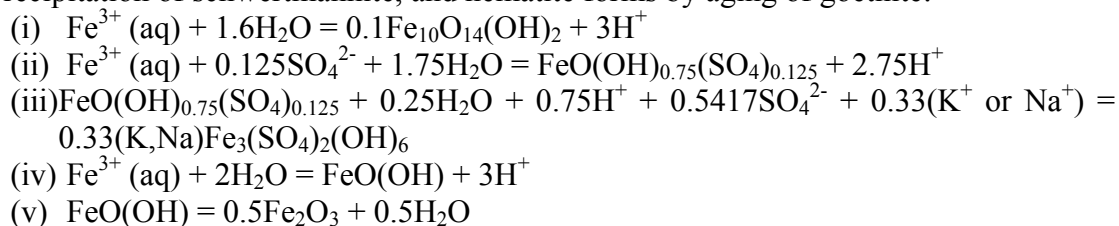
Finally, it is worth noting that our assumptions about a reaction pathway in which all  $\text{Fe}^{3+}$  initially precipitates as schwertmannite, and then matures to hematite or jarosite, is just one possible pathway to produce the observed  $\text{Fe}^{3+}$ -mineral distribution in outcrop (albeit, one that is permitted by both field relationships and experimental evidence, e.g., refs. 6,7,15). We performed our calculations assuming that the Fe3D3 component of Mössbauer spectra is composed entirely of schwertmannite. Ref. 4 reports that the Fe3D3 component could be one or a combination of nanophase superparamagnetic hematite or goethite, akaganeite, ferrihydrite, or schwertmannite. Therefore, it is pertinent to consider at least a few alternate reaction pathways to produce the observed  $\text{Fe}^{3+}$ -mineral distribution in outcrop, to test whether or not our  $\text{H}^+$ - $\text{SO}_4^{2-}$  production-consumption reactions would change dramatically.

For instance, if the Fe3D3 were composed entirely of nanophase goethite, the jarosite were a direct precipitate from solution, and the hematite was formed by aging (i.e., paragenetic maturation) of jarosite, we would have the following set of reactions:



For the formation of nanophase goethite, a cumulative  $\text{H}^+$  production of 2 moles is indicated, with 0 moles of  $\text{SO}_4^{2-}$  consumed ((r1 or r2)+ri). For the formation of jarosite as a direct solution phase precipitate, a cumulative  $\text{H}^+$  production of 1 mole is indicated, with 0.667 moles of  $\text{SO}_4^{2-}$  consumed ((r1 or r2)+rii). For the formation of hematite as a jarosite aging product, a cumulative  $\text{H}^+$  production of 2 moles is indicated, with 0 moles of  $\text{SO}_4^{2-}$  consumed ((r1 or r2)+rii+riii). The net acid production for this case is 5 moles  $\text{H}^+$ , and the net  $\text{SO}_4^{2-}$  consumption is 0.667 moles.

Similarly, for another set of reactions in which the Fe3D3 component is assumed to be ferrihydrite (chemical formula from ref. 16), the jarosite forms by dissolution-reprecipitation of schwertmannite, and hematite forms by aging of goethite:



For the formation of ferrihydrite, a cumulative  $\text{H}^+$  production of 2 moles is indicated, with 0 moles of  $\text{SO}_4^{2-}$  consumed ((r1 or r2)+ri). For the formation of jarosite by aging of schwertmannite, a cumulative  $\text{H}^+$  production of 1 mole is indicated, with 0.667 moles of  $\text{SO}_4^{2-}$  consumed ((r1 or r2)+rii+riii). For the formation of hematite as a goethite aging product, a cumulative  $\text{H}^+$  production of 2 moles is indicated, with 0 moles of  $\text{SO}_4^{2-}$  consumed ((r1 or r2)+riv+rv). The net acid production in this case is 5 moles  $\text{H}^+$ , and the net  $\text{SO}_4^{2-}$  consumption is 0.667 moles.

Finally, if the Fe3D3 component is assumed to be nanophase hematite and both the jarosite and non-Fe3D3 hematite are direct solution phase precipitates:

- (i)  $\text{Fe}^{3+}(\text{aq}) + 1.5\text{H}_2\text{O} = 0.5\text{Fe}_2\text{O}_3 (\text{Fe3D3}) + 3\text{H}^+$   
 (ii)  $\text{Fe}^{3+}(\text{aq}) + 0.667\text{SO}_4^{2-} + 0.33(\text{K}^+ \text{ or } \text{Na}^+) + 2\text{H}_2\text{O} = 0.33(\text{K,Na})\text{Fe}_3(\text{SO}_4)_2(\text{OH})_6 + 2\text{H}^+$   
 (iii)  $\text{Fe}^{3+}(\text{aq}) + 1.5\text{H}_2\text{O} = 0.5\text{Fe}_2\text{O}_3 + 3\text{H}^+$

For the formation of nanophase Fe<sub>3</sub>D<sub>3</sub> hematite, a cumulative H<sup>+</sup> production of 2 moles is indicated, with 0 moles of SO<sub>4</sub><sup>2-</sup> consumed ((r1 or r2)+ri). For the formation of jarosite as a direct solution phase precipitate, a cumulative H<sup>+</sup> production of 1 mole is indicated, with 0.667 moles of SO<sub>4</sub><sup>2-</sup> consumed ((r1 or r2)+rii). For the formation of non-Fe<sub>3</sub>D<sub>3</sub> (concretionary) hematite, a cumulative H<sup>+</sup> production of 2 moles is indicated, with 0 moles of SO<sub>4</sub><sup>2-</sup> consumed ((r1 or r2)+riii). The net acid production in this case is again 5 moles H<sup>+</sup>, and the net SO<sub>4</sub><sup>2-</sup> consumption is 0.667 moles.

For all three of these “alternative” cases, a calculation of acid production versus titration results in the same outcome: a net excess of acid produced relative to acid titrated between pH 2-4. We note that the same is true for the case in which all Fe is oxidized and precipitates to form schwertmannite with no subsequent reactions to form other, more paragenetically mature ferric mineral phases.

Finally, we have modeled the outcome of all reaction pathways substituting hydronium jarosite (H<sub>3</sub>O)Fe<sub>3</sub>(SO<sub>4</sub>)<sub>2</sub>(OH)<sub>6</sub> for the Na- and K-jarosite endmembers. We find a slight difference in the amount of acid ultimately produced when hydronium jarosite is substituted, owing to the fact that hydronium jarosite incorporates acid (in the form of H<sub>3</sub>O<sup>+</sup>) into its structure. For all cases, when hydronium jarosite is substituted for Na- or K-jarosite, the amount of acid produced changes by -0.33 moles H<sup>+</sup> per mole of Fe<sup>3+</sup> incorporated into hydronium jarosite. Despite this difference, the ultimate outcome is the same as that for K- or Na-jarosite: an excess of acid relative to available titrant.

## 2.0 IRON OXIDATION RATES

For our analysis of the rate of UV-promoted Fe-oxidation, we use equation (VI) of ref. 17 to determine the concentration of  $\text{Fe}^{3+}(\text{aq})$  as a function of time:

- $\text{Fe}^{3+}(\text{aq}) = ((1+2\text{BAI}_0t)^{1/2} - 1)/B$ ; (units of moles $\cdot\text{L}^{-1}$ )
- $A = 2 \cdot \text{Quantum Efficiency}$  - (unitless)
  - Quantum Efficiency =  $k_3/(k_2+k_3) = 0.075$
  - $k_1: \text{Fe}^{2+}(\text{aq}) + h\nu = \text{Fe}^{2+\cdot}(\text{aq})$ ; (photochemical excitation of  $\text{Fe}^{2+}(\text{aq})$ )
  - $k_2: \text{Fe}^{2+\cdot}(\text{aq}) = \text{Fe}^{2+}(\text{aq})$ ; (deactivation)
  - $k_3: \text{Fe}^{2+\cdot}(\text{aq}) + \text{H}_2\text{O} = \text{Fe}^{3+}(\text{aq}) + \text{OH}^- + 0.5\text{H}_2$ ; (oxidation)
- $I_0 = \text{Light intensity}$ ; (units of Einsteins $\cdot\text{L}^{-1}\cdot\text{min}^{-1}$ , 1 Einstein = 1 mole of photons)
- $t = \text{time}$ ; (units of min)
- $B = \epsilon\text{Fe}^{3+}/(\epsilon\text{Fe}^{2+}\cdot\text{Fe}^{2+}_0)$ ; (units of  $\text{L}\cdot\text{mol}^{-1}$ )
  - $\epsilon\text{Fe}^{3+} = \text{molar extinction coefficient} = 2850 \text{ mol}^{-1}\cdot\text{cm}^{-1}$
  - $\epsilon\text{Fe}^{2+} = \text{molar extinction coefficient} = 14.8 \text{ mol}^{-1}\cdot\text{cm}^{-1}$
  - $\text{Fe}^{2+}_0 = \text{Initial concentration of } \text{Fe}^{2+}(\text{aq})$ ; (units of moles $\cdot\text{L}^{-1}$ )
- Divide  $\text{Fe}^{3+}(\text{aq})$  by time (min) to determine a rate; (units of moles $\cdot\text{L}^{-1}\cdot\text{min}^{-1}$ )

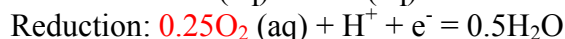
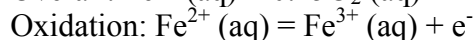
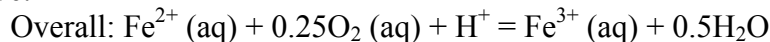
The rate was determined by ref. 17 at 20°C and 1 bar atmospheric pressure in de-oxygenated solutions having Fe-concentrations ranging from 20-100mM and pH=0.35 (0.8N  $\text{H}_2\text{SO}_4$ ). The UV light source was determined to output 90% of its total intensity at 2536Å<sup>17</sup>. Photon flux in their experiments was varied between  $1.84 \times 10^{-4}$  and  $4.59 \times 10^{-4}$  Einsteins $\cdot\text{L}^{-1}\cdot\text{min}^{-1}$ . Experiments conducted on de-oxygenated solutions at variable pH indicate that rates decrease by less than a factor of ~2 between pH 0.35 and 3.0<sup>18</sup>.

In order to more closely approximate conditions of photon flux and initial  $\text{Fe}^{2+}(\text{aq})$  concentration in a fluid at the martian surface, we assume an  $\text{Fe}^{2+}(\text{aq})$  concentration based on the experimental data of ref. 19 = 3.96mM. We further assume that the photon flux striking the surface of the Earth's oceans between 2000-3000Å is a reasonable first approximation, =  $0.03 \text{ Einsteins}\cdot\text{cm}^{-2}\cdot\text{yr}^{-1}$ <sup>20</sup>. We then convert this flux, which is expressed in units of area, to units of Einsteins $\cdot\text{L}^{-1}\cdot\text{min}^{-1}$  for use in equation (VI) of ref. 17, above. This is done by dividing the flux through by a fixed path length (L, in cm). We further reduce the intensity of the UV light for a given path length using an experimentally determined absorption coefficient for water at 2540Å ( $\alpha=0.00423644\text{cm}^{-1}$ ) and calculating the fractional transmittance of light at 2540Å using  $T=e^{-L\alpha}$ . Thus, we are able to determine a depth dependant rate for UV-promoted Fe-oxidation.

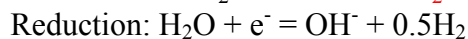
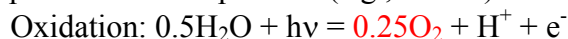
For our analysis of the rate of Fe-oxidation by dissolved  $\text{O}_2(\text{aq})$  we use the rate law of ref. 21, which is invariant below  $\text{pH} \leq 3.5-4.0$ . This rate law was determined experimentally at STP. We assume a dissolved  $\text{Fe}^{2+}(\text{aq}) = 3.96\text{mM}$ <sup>19</sup>. We then vary  $\text{O}_2$  pressure (atm) by fixing the abundance of  $\text{O}_2$  at 0.13%, which is the average  $\text{O}_2$  abundance in the present-day martian atmosphere<sup>22</sup>, and increasing total atmospheric pressure from the present-day value of ~10mbars to a maximum of 2000mbars, well within the total atmospheric pressures posited for early Mars<sup>23</sup>. The concentration of dissolved  $\text{O}_2(\text{aq})$  was then calculated using a 25°C Henry's Law constant of  $769 \text{ L}\cdot\text{atm}\cdot\text{mol}^{-1}$ .

### 3.0 H-ESCAPE RATE CALCULATIONS & SENSITIVITY ANALYSIS

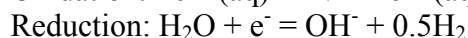
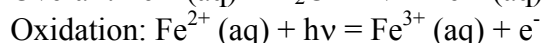
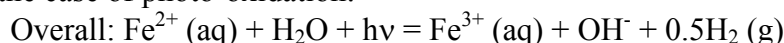
We recognize that for either Fe-oxidation reaction (below), 0.5 moles of H<sub>2</sub> is produced for every mole of Fe-oxidized. In the case of oxidation by molecular O<sub>2</sub>, we have:



In order to supply O<sub>2</sub> to the above reaction, a water oxidation-reduction reaction is required in which H<sub>2</sub>O is broken down and H<sub>2</sub> is produced, likely in the atmosphere in the presence of UV photons (e.g., ref. 24):



In the case of photo-oxidation:



To find the H-escape rate required to balance the H<sub>2</sub> produced by Fe-oxidation (**Figure 3** of the manuscript), we use the average number of moles of Fe<sup>3+</sup>/kg outcrop (**Table S1**, =1.84 ± 0.15 moles Fe<sup>3+</sup>/kg), recognizing that each mole of Fe<sup>3+</sup> is equivalent to 0.5 moles H<sub>2</sub> produced. We must then derive a value for the total number of moles of H<sub>2</sub> produced for the entire mass of Meridiani Planum outcrop for comparison to known or estimated values of planetary H-escape. In order to derive this value, we multiply the number of moles of H<sub>2</sub> produced/kg outcrop (=0.92 moles H<sub>2</sub>/kg) by an estimate of the total mass of Meridiani Planum outcrop, varying the thickness of the outcrop from 0-1000m, and setting all other variables equal to those shown on **Table S5**.

The outcrop thickness, and more importantly, how much of that vertical thickness is made up of materials equivalent to those examined by *Opportunity*, is probably the greatest source of uncertainty in our calculation of outcrop mass. *Opportunity* has observed ~30m of vertical stratigraphy having the same elemental and mineralogical composition as the analyses used in this report<sup>25</sup>. Estimates of total erosion based on observations of crater retention indicate the loss of ~10-80m of soft, sulfate-bearing sedimentary strata since the Hesperian period<sup>26</sup>. Therefore, 50-100 meters of material having the same or similar composition to the analyses used here is probably a reasonable minimum estimate of stratigraphic thickness. Orbital observations suggest that sulfate-bearing strata extend over ~800m of vertical thickness and ~2x10<sup>5</sup>km<sup>2</sup> area in the Terra Meridiani region<sup>27-30</sup>.

In order to provide a sense of the variation that might be caused by uncertainty in outcrop area, density, or porosity, we have performed a sensitivity analysis by varying outcrop thickness from 0-1000m, outcrop area from 1-4x10<sup>5</sup>km<sup>2</sup> (half and double the area estimated from orbit), porosity between 0 and 30% (encapsulating the full range of suggested porosity values, **Table S5**), and density between 2100kg/m<sup>3</sup> (opal) and 3000kg/m<sup>3</sup> (basalt), to arrive at a range of outcrop masses. From these mass ranges, we can determine a range in H<sub>2</sub> production resulting from Fe-oxidation. The results of this

sensitivity analysis are shown on **Figure S2**. As shown, for any particular thickness of outcrop, less than one order of magnitude variation in H<sub>2</sub> production is observed for variations in outcrop area, porosity, or density.

*Note: All calculations used in this paper are available on request from the corresponding author as .xls files.*

## REFERENCES:

- 1 Gellert, R. & Rieder, R. MER APXS Oxide Abundance Archive, NASA Planetary Data System, MER1/MER2-M-APXS-5-OXIDE-SCI-V1.0 (MER APXS Oxide Abundance Archive, NASA Planetary Data System, MER1/MER2-M-APXS-5-OXIDE-SCI-V1.0, 2006).
- 2 Rieder, R. *et al.*, Chemistry of Rocks and Soils at Meridiani Planum from the Alpha Particle X-ray Spectrometer. *Science* **306**, 1746-1749 (2004).
- 3 Klingelhofer, G. *et al.*, Jarosite and Hematite at Meridiani Planum from Opportunity's Mossbauer Spectrometer. *Science* **306**, 1740-1745 (2004).
- 4 Morris, R.V. *et al.*, Mossbauer mineralogy of rock, soil, and dust at Meridiani Planum, Mars: Opportunity's journey across sulfate-rich outcrop, basaltic sand and dust, and hematite lag deposits. *Journal of Geophysical Research* **111**, E12S15, doi: 10.1029/2006JE002791 (2006).
- 5 Knoll, A.H. *et al.*, Veneers, rinds, and fracture fills: Relatively late alteration of sedimentary rocks at Meridiani Planum, Mars. *Journal of Geophysical Research-Planets* **113**, E06S16, doi:10.1029/2007JE002949 (2008).
- 6 Bigham, J.M. & Nordstrom, D.K., Iron and Aluminum Hydroxysulfates from Acid Sulfate Waters in *Sulfate Minerals*, edited by C.N. Alpers, J.L. Jambor, & D.K. Nordstrom (Mineralogical Society of America, Washington D.C., 2000), Vol. 40, pp. 351-403.
- 7 Tosca, N., McLennan, S., Dyar, M., Sklute, E., & Michel, F., Fe oxidation processes at Meridiani Planum and implications for secondary Fe mineralogy on Mars. *Journal of Geophysical Research* **113**, doi:10.1029/2007JE003019, 002008 (2008).
- 8 Burns, R.G. & Fisher, D.S., Iron-sulfur mineralogy of Mars - Magmatic evolution and chemical-weathering products. *Journal of Geophysical Research* **95**, 14415-14421 (1990).
- 9 Madden, M.E.E., Bodnar, R.J., & Rimstidt, J.D., Jarosite as an indicator of water-limited chemical weathering on Mars. *Nature* **431**, 821-823 (2004).
- 10 King, P.L. & McSween Jr, H.Y., Effects of H<sub>2</sub>O, pH, and oxidation state on the stability of Fe-minerals on Mars. *Journal of Geophysical Research* **110**, E12S10, doi:10.1029/2005JE002485, 002005 (2005).
- 11 Burns, R.G., Rates and mechanisms of chemical weathering of ferromagnesian silicate minerals on Mars. *Geochimica et Cosmochimica Acta* **57**, 4555-4574 (1993).
- 12 Burns, R.G. & Fisher, D.S., Rates of oxidative weathering on the surface of Mars. *Journal of Geophysical Research* **98**, 3365-3372 (1993).
- 13 Clark, B.C. *et al.*, Chemistry and mineralogy of outcrops at Meridiani Planum. *Earth and Planetary Science Letters* **240**, 73-94 (2005).
- 14 Glotch, T.D. *et al.*, Mineralogy of the light-toned outcrop at Meridiani Planum as seen by the Miniature Thermal Emission Spectrometer and implications for its formation. *Journal of Geophysical Research* **111**, E12S03, doi:10.1029/2005JE002672 (2006).
- 15 Hammarstrom, J.M., Seal II, R.R., Meier, A.L., & Kornfeld, J.M., Secondary sulfate minerals associated with acid drainage in the eastern U.S.: recycling of

- metals and acidity in surficial environments. *Chemical Geology* **215**, 407-431 (2005).
- 16 Michel, F.M. *et al.*, The Structure of Ferrihydrite, a Nanocrystalline Material. *Science* **316**, 1726-1729 (2007).
- 17 Jortner, J. & Stein, G., Photochemical evolution of hydrogen from aqueous solutions of ferrous ions.1. Reaction mechanism at low pH. *Journal of Physical Chemistry* **66**, 1258-1264 (1962).
- 18 Jortner, J. & Stein, G., Photochemical evolution of hydrogen from aqueous solutions of ferrous ions.2. Effect of changing pH. *Journal of Physical Chemistry* **66**, 1264-1271 (1962).
- 19 Tosca, N.J. & McLennan, S.M., Experimental constraints on the evaporation of partially oxidized acid-sulfate waters at the martian surface. *Geochimica et Cosmochimica Acta* **73**, 1205-1222 (2009).
- 20 Cairns-Smith, A.G., Precambrian solution photchemistry, inverse segregation, and banded iron formations. *Nature* **276**, 807-808 (1978).
- 21 Singer, P.C. & Stumm, W., Acidic mine drainage: the rate determining step *Science* **167**, 1121-1123 (1970).
- 22 Owen, T., The Composition and Early History of the Atmosphere of Mars in *Mars*, edited by HH Kieffer, BM Jakosky, CW Snyder, & MS Mathews (University of Arizona Press, Tucson, 1992), pp. 818-834.
- 23 Jakosky, B.M. & Phillips, R.J., Mars' volatile and climate history. *Nature* **412**, 237-244 (2001).
- 24 Yung, Y.L. *et al.*, HDO in the martian atmosphere - Implications for the abundance of crustal water. *Icarus* **76**, 146-159 (1988).
- 25 Squyres, S.W. *et al.*, Exploration of Victoria Crater by the Mars Rover Opportunity. *Science* **324**, 1058-1061 (2009).
- 26 Golombek, M.P. *et al.*, Erosion rates at the Mars Exploration Rover landing sites and long-term climate change on Mars. *Journal of Geophysical Research* **111**, E12S10, doi:10.1029/2006JE002754 (2006).
- 27 Arvidson, R.E. *et al.*, Spectral Reflectance and Morphologic Correlations in Eastern Terra Meridiani, Mars. *Science* **307**, 1591-1594 (2005).
- 28 Hynek, B.M. & Phillips, R.J., The stratigraphy of Meridiani Planum, Mars, and implications for the layered deposits' origin. *Earth and Planetary Science Letters* **274**, 214-220 (2008).
- 29 Arvidson, R.E. *et al.*, Nature and origin of the hematite-bearing plains of Terra Meridiani based on analyses of orbital and Mars Exploration rover data sets. *Journal of Geophysical Research-Planets* **111**, E12S08, doi:10.1029/2006JE002728, 002006 (2006).
- 30 Hynek, B.M., Arvidson, R.E., & Phillips, R.J., Geologic setting and origin of Terra Meridiani hematite deposit on Mars. *Journal of Geophysical Research* **107**, 5088, doi:10.1029/2002JE001891 (2002).
- 31 McLennan, S.M. *et al.*, Provenance and diagenesis of the evaporite-bearing Burns formation, Meridiani Planum, Mars. *Earth and Planetary Science Letters* **240**, 95-121 (2005).

- <sup>32</sup> Tosca, N.J. *et al.*, Geochemical Modeling of Evaporation Processes on Mars: Insight from the Sedimentary Record at Meridiani Planum. *Earth and Planetary Science Letters* **240**, 122-148 (2005).

**Table S1: APXS and Mössbauer Data Used for Titration Calculations**

	APXS Analysis Name, Sol # <sup>1</sup>	FeO	SO <sub>3</sub>	P <sub>2</sub> O <sub>5</sub>	Cl	Fe	SO <sub>4</sub>	PO <sub>4</sub>	Cl	OI	Pyx	Jar	Hm	Fe3D3
1	McKittrick RAT, 31	16.5	21.3	0.99	0.60	2.30	2.66	0.14	0.17	1	12	26	39	22
2	Guadalupe RAT, 36	14.8	24.9	0.97	0.50	2.06	3.11	0.14	0.14	1	9	38	36	16
3	Mojo2 RAT, 45	15.3	23.6	1.01	0.54	2.13	2.95	0.14	0.15	1	15	22	38	25
4	Golf Post RAT FRAM, 87	15.7	25.2	0.97	0.66	2.19	3.15	0.14	0.18	0	10	33	37	20
5	LionStone Numa RAT, 108	14.3	22.8	1.01	0.91	1.99	2.85	0.14	0.26	1	14	30	34	22
6	Kentucky Cobble Hill2 RAT, 145	14.7	24.4	1.05	0.65	2.05	3.04	0.15	0.18	1	15	28	35	20
7	Virginia RAT, 147	15.5	22.1	1.07	0.60	2.16	2.76	0.15	0.17	2	16	28	35	19
8	Ontario London RAT, 149	14.5	23.7	1.11	0.72	2.02	2.96	0.16	0.20	1	18	27	35	19
9	Grindstone RAT, 153	14.8	21.5	1.07	1.45	2.06	2.68	0.15	0.41	2	17	28	34	20
10	Kettlestone RAT, 155	15.2	23.0	1.03	1.75	2.12	2.88	0.15	0.49	2	15	29	32	21
11	millstone Dramensfjord RAT, 162	15.8	21.1	1.17	1.98	2.20	2.64	0.16	0.56	1	21	27	33	18
12	Diamond Jenness Holman3 RAT <sup>3</sup>	15.5	19.6	1.06	1.50	2.15	2.45	0.15	0.42	2	11	29	41	18
13	MacKenzie Campell RAT, 184	15.6	17.0	1.15	1.90	2.17	2.12	0.16	0.54	1	15	31	34	19
14	Inuvik Toruyuktuk RAT, 187	17.1	18.2	1.11	1.67	2.38	2.27	0.16	0.47	2	14	26	40	18
15	Bylot RAT, 195	17.7	19.3	1.01	1.69	2.46	2.41	0.14	0.48	2	13	30	41	14
16	Escher Kirchner RAT, 220	15.7	23.0	1.01	0.78	2.19	2.88	0.14	0.22	1	15	30	35	20
17	Wharenhui RAT, 312	15.1	21.3	1.08	1.49	2.10	2.66	0.15	0.42	5	14	28	34	19
18	Gagarin RAT, 403	15.9	28.6	1.07	0.61	2.21	3.57	0.15	0.17	1	7	32	37	24
19	IceCream RAT, 548	15.8	23.8	1.04	0.64	2.20	2.97	0.15	0.18	3	10	32	36	19

<sup>1</sup> Represents the martian day (or sol) of the *Opportunity* mission on which the APXS analysis was collected.

<sup>2</sup> Percentage of Fe-atoms associated with each phase, where OI=olivine, Pyx=pyroxene, Jar=jarosite, Hm=hematite, and Fe3D3=schwertmannite.

<sup>3</sup> Represents the average of data reported for analyses collected on the same target on sols 178 and 180.

**Table S2: Acid Produced and Sulfate Consumed by Reactions 3-6 following Fe-oxidation**

	H <sup>+</sup> Produced				SO <sub>4</sub> <sup>2-</sup> Consumed			
	Moles H <sup>+</sup> /kg Outcrop				Moles SO <sub>4</sub> <sup>2-</sup> /kg Outcrop			
	R3 (schwert)	R3+R5+R6 (hematite)	R3+R4 (jarosite)	Tot	R3 (schwert)	R3+R5+R6 (hematite)	R3+R4 (jarosite)	Total
1	0.88	1.79	0.60	<b>3.27</b>	0.06	0.00	0.40	<b>0.46</b>
2	0.58	1.48	0.78	<b>2.84</b>	0.04	0.00	0.52	<b>0.56</b>
3	0.93	1.62	0.47	<b>3.02</b>	0.07	0.00	0.31	<b>0.38</b>
4	0.76	1.62	0.72	<b>3.10</b>	0.05	0.00	0.48	<b>0.54</b>
5	0.77	1.35	0.60	<b>2.72</b>	0.05	0.00	0.40	<b>0.45</b>
6	0.72	1.43	0.57	<b>2.72</b>	0.05	0.00	0.38	<b>0.43</b>
7	0.72	1.51	0.60	<b>2.83</b>	0.05	0.00	0.40	<b>0.45</b>
8	0.67	1.41	0.54	<b>2.63</b>	0.05	0.00	0.36	<b>0.41</b>
9	0.72	1.40	0.58	<b>2.70</b>	0.05	0.00	0.38	<b>0.44</b>
10	0.78	1.35	0.61	<b>2.75</b>	0.06	0.00	0.41	<b>0.46</b>
11	0.69	1.45	0.59	<b>2.74</b>	0.05	0.00	0.40	<b>0.45</b>
12	0.68	1.76	0.62	<b>3.06</b>	0.05	0.00	0.42	<b>0.46</b>
13	0.72	1.48	0.67	<b>2.87</b>	0.05	0.00	0.45	<b>0.50</b>
14	0.75	1.90	0.62	<b>3.27</b>	0.05	0.00	0.41	<b>0.47</b>
15	0.60	2.02	0.74	<b>3.36</b>	0.04	0.00	0.49	<b>0.54</b>
16	0.76	1.53	0.66	<b>2.95</b>	0.05	0.00	0.44	<b>0.49</b>
17	0.70	1.43	0.59	<b>2.71</b>	0.05	0.00	0.39	<b>0.44</b>
18	0.93	1.64	0.71	<b>3.28</b>	0.07	0.00	0.47	<b>0.54</b>
19	0.73	1.58	0.70	<b>3.02</b>	0.05	0.00	0.47	<b>0.52</b>
								SO <sub>4</sub> <sup>2-</sup> Remaining
								2.20
								2.55
								2.57
								2.61
								2.40
								2.61
								2.30
								2.55
								2.25
								2.41
								2.19
								1.99
								1.62
								1.80
								1.88
								2.38
								2.22
								3.03
								2.45

**Table S3: Results of pH = 2 Titration Calculation**

		Species Distribution at pH = 2														Acid Remaining
		Moles/kg Outcrop														Moles H <sup>+</sup> /kg Outcrop
		H <sub>2</sub> SO <sub>4</sub>	HSO <sub>4</sub> <sup>-</sup>	SO <sub>4</sub> <sup>2-</sup>	HCl	Cl <sup>-</sup>	H <sub>3</sub> PO <sub>4</sub>	H <sub>2</sub> PO <sub>4</sub> <sup>-</sup>	HPO <sub>4</sub> <sup>2-</sup>	PO <sub>4</sub> <sup>3-</sup>	H <sub>2</sub> CO <sub>3</sub>	HCO <sub>3</sub> <sup>-</sup>	CO <sub>3</sub> <sup>2-</sup>			
1	1.10E-04	1.07	1.13	1.27E-02	5.94	8.07E-02	5.88E-02	3.71E-07	1.65E-17	0.23	1.04E-05	4.88E-14	<b>1.36</b>			
2	1.28E-04	1.24	1.30	1.52E-02	7.13	7.91E-02	5.76E-02	3.63E-07	1.62E-17	0.23	1.04E-05	4.88E-14	<b>0.76</b>			
3	1.29E-04	1.25	1.32	1.40E-02	6.53	8.23E-02	6.00E-02	3.78E-07	1.69E-17	0.23	1.04E-05	4.88E-14	<b>0.92</b>			
4	1.31E-04	1.28	1.34	1.16E-02	5.42	7.91E-02	5.76E-02	3.63E-07	1.62E-17	0.23	1.04E-05	4.88E-14	<b>1.00</b>			
5	1.20E-04	1.17	1.23	8.32E-03	3.89	8.23E-02	6.00E-02	3.78E-07	1.69E-17	0.23	1.04E-05	4.88E-14	<b>0.70</b>			
6	1.31E-04	1.27	1.34	1.17E-02	5.48	8.56E-02	6.24E-02	3.93E-07	1.75E-17	0.23	1.04E-05	4.88E-14	<b>0.59</b>			
7	1.16E-04	1.12	1.18	1.27E-02	5.94	8.72E-02	6.36E-02	4.01E-07	1.79E-17	0.23	1.04E-05	4.88E-14	<b>0.84</b>			
8	1.28E-04	1.24	1.31	1.06E-02	4.93	9.05E-02	6.59E-02	4.16E-07	1.85E-17	0.23	1.04E-05	4.88E-14	<b>0.50</b>			
9	1.13E-04	1.10	1.15	5.22E-03	2.44	8.72E-02	6.36E-02	4.01E-07	1.79E-17	0.23	1.04E-05	4.88E-14	<b>0.74</b>			
10	1.21E-04	1.18	1.23	4.35E-03	2.03	8.40E-02	6.12E-02	3.86E-07	1.72E-17	0.23	1.04E-05	4.88E-14	<b>0.72</b>			
11	1.10E-04	1.07	1.12	3.84E-03	1.80	9.54E-02	6.95E-02	4.38E-07	1.95E-17	0.23	1.04E-05	4.88E-14	<b>0.77</b>			
12	9.97E-05	0.97	1.02	5.05E-03	2.36	8.60E-02	6.27E-02	3.95E-07	1.76E-17	0.23	1.04E-05	4.88E-14	<b>1.24</b>			
13	8.14E-05	0.79	0.83	3.99E-03	1.87	9.37E-02	6.83E-02	4.31E-07	1.92E-17	0.23	1.04E-05	4.88E-14	<b>1.19</b>			
14	9.04E-05	0.88	0.92	4.56E-03	2.13	9.05E-02	6.59E-02	4.16E-07	1.85E-17	0.23	1.04E-05	4.88E-14	<b>1.52</b>			
15	9.42E-05	0.92	0.96	4.49E-03	2.10	8.23E-02	6.00E-02	3.78E-07	1.69E-17	0.23	1.04E-05	4.88E-14	<b>1.61</b>			
16	1.20E-04	1.16	1.22	9.77E-03	4.57	8.23E-02	6.00E-02	3.78E-07	1.69E-17	0.23	1.04E-05	4.88E-14	<b>0.94</b>			
17	1.11E-04	1.08	1.14	5.08E-03	2.38	8.80E-02	6.42E-02	4.04E-07	1.80E-17	0.23	1.04E-05	4.88E-14	<b>0.76</b>			
18	1.52E-04	1.48	1.55	1.24E-02	5.78	8.72E-02	6.36E-02	4.01E-07	1.79E-17	0.23	1.04E-05	4.88E-14	<b>0.93</b>			
19	1.23E-04	1.20	1.26	1.19E-02	5.55	8.48E-02	6.18E-02	3.89E-07	1.74E-17	0.23	1.04E-05	4.88E-14	<b>0.97</b>			



**Table S5: Values used for estimate of Meridiani Planum outcrop mass**

Parameter	Value	Reference(s)	Comment
Area	$2 \times 10^5 \text{ km}^2$	28	
Thickness	0-1000m	27-30	
Porosity	15%	31,32	Intermediate between a modeled upper limit of 30% <sup>32</sup> and images demonstrating that there are portions of outcrop with essentially zero visible porosity <sup>31</sup> .
Density	$2310 \text{ kg/m}^3$	none	This is the density of gypsum

**Figure S1:** Bjerrum diagrams showing the speciation of base anions as a function of pH for  $S^{6+}$  and  $C^{4+}$  species (Figure S1A) and  $P^{5+}$  and  $Cl^-$  species (Figure S1B). The stability range for jarosite, pH = 2-4, is shown for reference. The calculations were performed for total individual base ion concentrations of  $10^{-2}$  mole/L, but we note that the relative abundances determined by speciation are dependant only on pH (i.e., relative abundances are independent of total concentration).

**Figure S2:**  $H_2$  production (moles) resulting from Fe-oxidation plotted as a function of outcrop thickness for various estimates of the area, porosity, and density of Meridiani Planum outcrop. On the lower two panels, the uppermost line corresponds to estimates made assuming a basalt outcrop density ( $3000 \text{ kg/m}^3$ ), followed by gypsum ( $2310 \text{ kg/m}^3$ ), and opal ( $2100 \text{ kg/m}^3$ ).

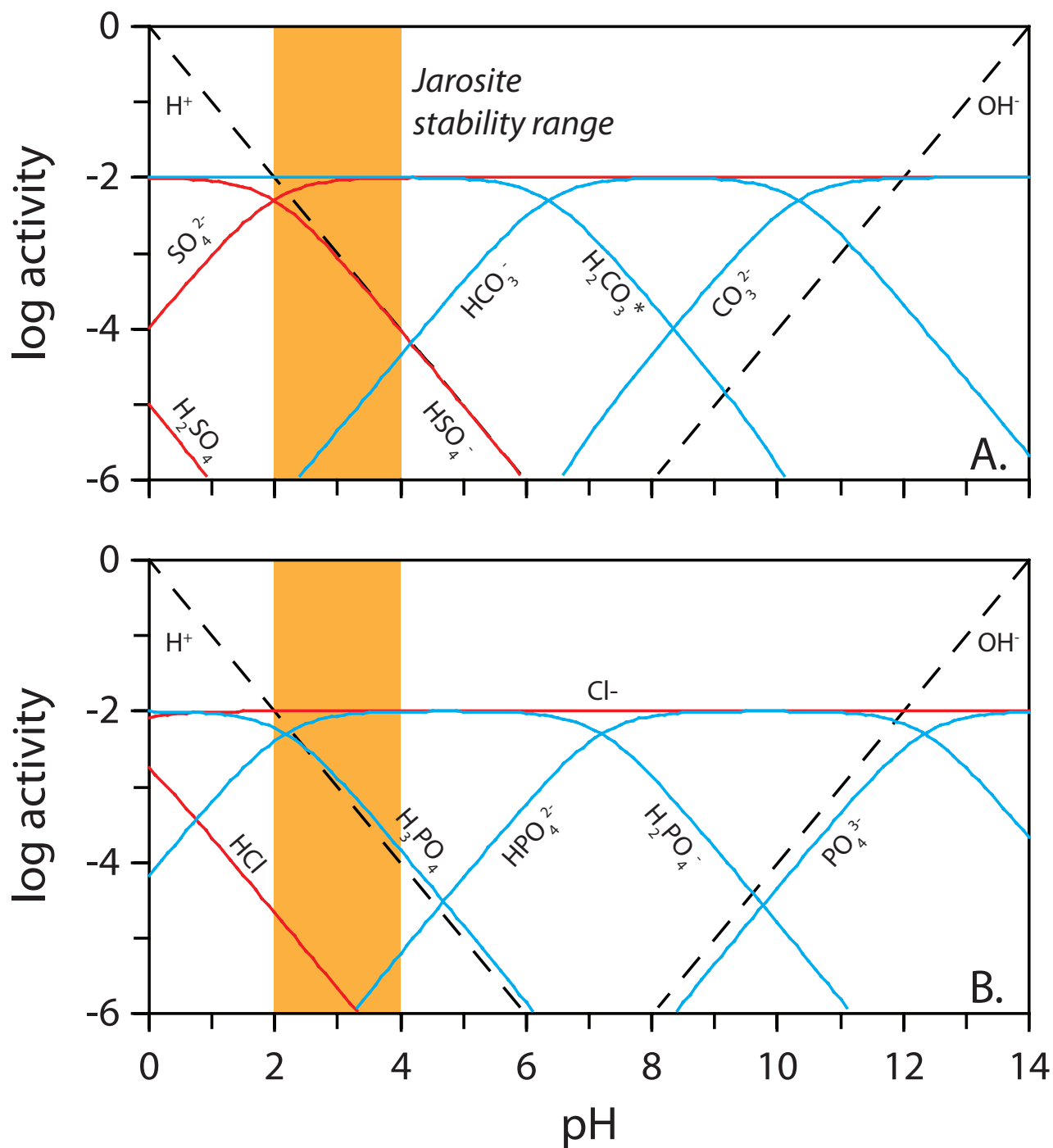


Figure S1

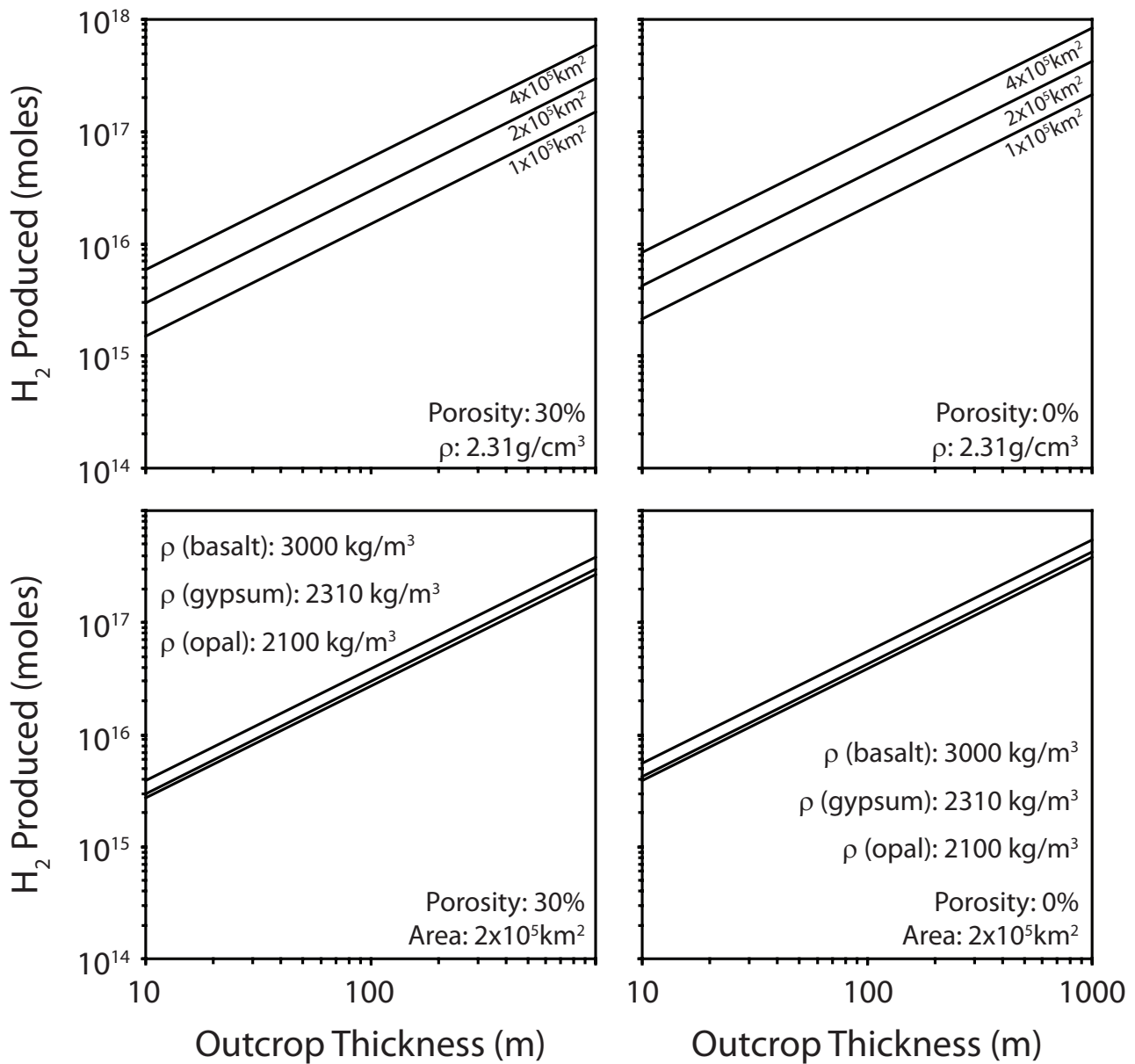


Figure S2